

Materials design based on a material-motif network and heterogeneous graphs

Anoj Aryal¹, Dr. Weiyi Gong¹, Dr. Huta Banjade², Prof. Qimin Yan¹

¹Department of Physics, Northeastern University, Boston, MA 02115, USA

²Department of Physics, Virginia Commonwealth University, VA 23284, USA

Keywords: *motif-based materials network, functional motifs, materials screening, property prediction*

Machine learning models for functional materials design require precise and informative representations of material systems. Common representations encode atomic composition and bonding but often do not include local coordination environments across chemically diverse crystals. Recurring structural motifs provide a motif-level description of crystalline solids and can serve as interpretable descriptors for structure–property learning. To analyze the motif connectivity in materials, a bipartite material–motif network is constructed from 131,548 Materials Project entries, with materials and motifs as the two node sets. Edges connect materials to their constituent motifs and are weighted by motif distortion, which quantifies the strength of each material–motif association. Network connectivity is analyzed to identify motif-defined material clusters that capture recurring local geometries relevant to structure–property trends. Most shared motifs act as hubs that connect otherwise disconnected regions of the network, enabling motif-guided screening by expanding from known motifs to nearby materials in the same neighborhoods. A network-embedding step converts this weighted connectivity into vector representations of materials. Using these motif-informed embeddings, property prediction yields a formation energy mean absolute error (MAE) of $0.157\text{ eV atom}^{-1}$ and a bandgap MAE of 0.601 eV . These results indicate that motif connectivity provides a compact, interpretable representation that complements existing descriptors for scalable screening and structure–property modeling.

1 Introduction

The data-driven design and discovery of novel materials in materials science has been advanced by the availability of large-scale databases generated through high-throughput first-principles calculations.[1, 2, 3, 4] Existing materials discovery workflows adopt multi-tier screening strategies in which candidate materials are filtered based on physical descriptors such as elemental composition, crystal symmetry, and stability, followed by computationally expensive density functional theory (DFT) calculations. These data-driven workflows have been used to identify candidates with promising applications in energy storage, photocatalysis, and photovoltaics. However, explicit incorporation of structural similarity between materials remains relatively uncommon, despite the strong correlation between the local atomic arrangements and material properties. Local atomic environments could therefore serve as powerful screening criteria in materials discovery, complementing property-based approaches.

Integrating such relationships into scalable workflows requires an effective framework for representing and analyzing material connectivity. Network-based approaches have shown strong potential in capturing hidden relationships in complex real-world systems, including user-location interactions in social networks,[5] transit-hub connectivity in transportation networks,[6, 7] and protein-disease networks that support targeted drug discovery in molecular biochemistry.[8, 9] In materials science, previous studies have identified structural similarities and functional trends across materials based on features such as density of states, chemical similarities, and structure fingerprints.[10, 11, 12] However, the direct use of local coordination environments in a network-driven framework remains largely unexplored.

Local atomic environments or structure motifs describe the arrangement of atoms around a central site and form recurring building blocks in crystalline solids that strongly correlate with physical, electronic, magnetic, and optical properties. They provide a chemically interpretable and symmetry-aware basis for representing structure–property relationships. Previously, motifs have been used to explore application specific trends; for example, TiO_6 octahedra in perovskites and VO_4 tetrahedra in bismuth-based compounds have been associated with optoelectronic properties relevant to solar energy conversion.[13, 14] Similarly,

in superconductors, Cu–O planes and CuO₄ square-planar motifs in cuprates and FeAs₄ tetrahedra in iron-based compounds are central to the emergence of high- T_c behavior.[15, 16, 17] Structure motif analysis has also been used to assess crystal similarity within the Materials Project database.[1, 18, 19, 20, 21] These examples highlight the potential of motifs as a compact yet informative representation of crystal structure.

A systematic framework for capturing the material–motif relationships can be modeled within a network graph structure where materials and motifs can be encoded as a separate set of nodes and their connectivity as edges. Network science offers a rich set of methodologies, such as random walks, centrality metrics, and graph embeddings, for analyzing both homogeneous and heterogeneous network structures. While early embedding methods focused on homogeneous networks,[22, 23] many real-world systems are heterogeneous.[24, 25, 26] In heterogeneous networks, bipartite learning approaches are effective for modeling two-type node relationships and for extracting informative low-dimensional representations for downstream tasks.[27, 28, 29] In parallel, machine learning (ML) models, particularly graph neural networks used in crystalline solids, have shown strong predictive performance representing crystal structure as a graph with atoms as nodes and bonds as edges.[30, 31, 32, 33, 34, 35, 36] For better representation of motifs in crystals, motif-based crystal graph with explicitly encoded motif-level features, along with atomic and bonding information has been used as input in machine learning model for predicting electronic bandgap and classifying materials as metals or non-metals.[37] In molecular chemistry, a similar strategy has been used to construct motif-based heterogeneous graph network and generate motif-level feature representations, which enrich molecular representation.[38]

In this work, a bipartite network connecting materials to their structure motifs is constructed, providing a systematic framework for capturing structural similarities across materials with common motifs. The connectivity encoded in the network is analyzed using the centrality metrics to identify clusters of related materials, offering a motif-centric perspective for guiding candidate selection in materials design workflows. In addition, this analysis reveals functional clusters of materials linked through characteristic motifs, such as VO₄ and TiO₆ in solar energy conversion, FeAs₄ and CuO₄ in superconductors, and NaO₆, MnO₆, and PO₄ in battery electrodes. These clusters not only highlight known functional compounds but also point to other materials that show similar functionality. A bipartite network embedding method[27] is applied to learn low-dimensional vector representations of materials (and motifs). For materials, the learned embeddings serve as enriched feature vectors that capture motif-based structure relationships. These representations are then used to predict key material properties such as formation energy and bandgap, and metal–nonmetal classification. The results demonstrate that a motif-informed bipartite network is effective in exploring the connectivity of structurally and functionally similar materials. The learned embeddings can be used as descriptors for materials and provide insights into the role of structure motifs in determining different properties. More importantly, this framework can be integrated into existing materials discovery workflows as an intermediate screening stage to enable the identification of candidate compounds with desired structure motifs with known functional applications.

2 Methods

2.1 Structure Motif Identification

Structure motifs are basic crystal-structure descriptors that provide chemically interpretable descriptors for structure–property relationships. For large datasets, a robust, automated procedure is required to extract motif information. Motifs are identified using a nearest-neighbor approach by analyzing each cation with its surrounding anions. The automated coordination environment analysis tool, developed by Waroquiers *et al.*[20] and implemented within the **ChemEnv** subpackage in pymatgen,[21] is used to generate the dataset for materials with motif information. However, not all identified motifs are perfect, as distortions are expected. The continuous symmetry measure (CSM)[39] is used to quantify the similarity of each polyhedron to the closest ideal IUPAC-defined geometry;[40] CSM = 0 corresponds to a perfect

environment, and larger values indicate increasing distortion. Motif nodes are initialized with one-hot encoding of motif type and atomic species, whereas material nodes are initialized with a one-hot encoding of atomic composition.

2.2 Material-Motif Bipartite Network

A bipartite graph $G(U, V, E)$, where U and V are the two distinct sets of nodes and E is the set of edges, is defined such that $U \cap V = \emptyset$. For example, in a user-item interaction, U represents the set of users and V represents the set of items. Each edge $E = U \times V$ connects a node in set U to a node in set V , indicating a particular user’s interaction with a specific item. Bipartite graphs offer a unique and rich structure to represent interactions between two distinct sets of entities. In bipartite network embedding, the goal is not only to model the observed edges between the different sets of nodes but also to capture the transitive relations within the same set of nodes.

Bipartite network embedding (BiNE)[27] is one such model to generate embedding vectors for bipartite graphs, which not only captures the relationship between two different sets of nodes defined as explicit relations but also captures transitive links within the same set of nodes, defined as implicit relations. In the structure motif-based network, materials and motifs are defined as two distinct sets of nodes. An edge is created between a material and a motif if that motif occurs in the material. Each motif node is treated as an ideal motif and the geometric distortions from ideal coordination geometries are quantified using the CSM. The edge weight is defined based on CSM, assigning weight = 1 to an undistorted motif with $CSM = 0$ while more distorted motifs have larger CSM and therefore smaller weights. The explicit relation is defined using this edge weight, which directly links a material to its constituent motifs. For implicit relations, the neighborhood information for each node based on transitive relationships within the network is used. For each material node, the first-order neighbors of the same node type are determined by its indirect connections to other materials linked by the same motifs. These neighbors are further refined by sorting based on degree centrality to prioritize highly connected and structurally significant nodes in the graph. To reduce redundancy, previously included neighbors are excluded from subsequent contexts, allowing each material node to have a focused and non-redundant representation of its relationships. Learning to predict these relationships produces dense vector representations that encode both explicit and implicit patterns in the bipartite network, enabling downstream tasks such as property prediction and classification. The model jointly optimizes both relation types and generates the embeddings for both node sets in the bipartite network.

From the material-motif dataset, a bipartite network is built with one node set for materials and the other for motifs. The bipartite network is used to visualize the material space, identify patterns, and explore different material families with various applications. The networkx package[41] is used to construct the network and compute centrality measures for network analyses. Gephi[42] and Cytoscape[43] are used for network visualization. Embedding vectors for the materials and motifs are then generated and used as input features for a neural network architecture to predict material properties (e.g., formation energy, bandgap) and for classification of metals and non-metals. The predictor is a feed-forward network with a fully connected hidden layer: inputs are projected to a 64-dimensional hidden space, followed by ReLU nonlinearity, and a final fully connected output layer. This sequential mapping enables effective feature transformation for regression and classification.

3 Results and Discussion

The materials used in this study are sourced from the Materials Project database.[1] From the processed dataset containing materials and associated motif information, a bipartite network is constructed where one node set represents materials and the other represents the structure motifs. The largest network consists of 131,548 materials from the Materials Project database, filtered to include entries with well-defined structure

motifs and no more than 50 atomic sites. In addition, two perovskite-specific networks are studied: one derived from the Matbench dataset[44] and the other from the MP database. The overall connectivity of the network can be characterized by the network density, which measures the network's total actual edges as a proportion of all possible edges. The network of materials from the MP database is sparse, with a density of 0.00003. This low density is expected because of the vast chemical and structural diversity of materials, such that each motif is compatible with only a limited subset of materials. As a result, the network exhibits only a small number of actual, physically meaningful material-motif associations out of all possible pairs.

In **Figure 1**, a representative subgraph is presented consisting of several complex metal oxides and their motifs to visualize the structural relationships captured in the network. Shared motifs appear as hubs connecting multiple materials, revealing clusters of structurally similar compounds. Such connectivity patterns can be analyzed to identify material families with comparable local structures, which may exhibit similar functional properties. In this way, the resulting network captures explicit structural relationships by linking materials through shared motifs. To examine the structural topology of this network, various standard centrality measures are computed and analyzed.

3.1 Centrality Measures

Centrality measures quantify the structural importance of individual nodes within a network. In the context of a material-motif bipartite network, these metrics allow for the identification of structurally significant materials or motifs. They reveal which nodes function as hubs or bridges, thereby shaping connectivity within the network. Materials with different structures and functionalities can be linked if they share motifs. Various centrality metrics are considered to assess the network's structure and identify nodes that are central to different clusters. **Table 1** summarizes the mean centrality measures for materials and motifs in different networks studied. All centrality values shown are computed on the undirected material-motif network with projected networks of materials and motifs. The results show that the graphs are sparse, heavy-tailed, and exhibit hub-bridge structure which is similar to that observed in human-virus protein-protein interaction (HV PPI) network.[45]

Degree is a local measure of how many direct connections a node has in a graph. In a material-motif bipartite network, a material's degree is equal to the number of motifs it contains, and a motif's degree is equal to the number of materials it appears in. In large sparse networks, the distribution of degree values is heavy-tailed, approximately following a power law.[46] As observed in **Figure 2a**, a small set of nodes has high degree while most nodes have small degree and connect to only a few other nodes. Degree centrality is the normalized form of degree, and identifies nodes involved in a large number of structural associations. The node with the highest degree centrality in the network is the PO_4 tetrahedral motif, which is also the most common motif in the dataset. Other frequently observed octahedral motifs MnO_6 , LiO_6 and FeO_6 also have higher degree centrality values as shown in Table S1. These motifs are effective in establishing connections among structurally dissimilar materials MnPO_4 , MnO , LiPO_3 , and $\text{Li}_3\text{Ti}_2(\text{PO}_4)_3$ thereby enhancing the overall connectivity of the network.

Clustering coefficient reflects the tendency of nodes to form local communities and is defined as the ratio of the number of edges actually present among its neighbors to the number of all possible edges among those neighbors. The network has a moderately high clustering coefficient (0.201) for materials from the MP database, indicating the presence of densely connected structural nodes within local subgraphs. Nodes with high degree tend to exhibit low clustering as observed in Table S1, because they connect many otherwise weakly related neighbors. The clustered structure of materials in the network is visualized in Figure 2b, where the clustering coefficient histogram highlights the prevalence of locally clustered regions. For example, material MnPO_4 is linked with other materials such as NaVPO_5 and $\text{Li}_3\text{V}_2(\text{PO}_4)_3$ because of the PO_4 motif and forms a material cluster with other similarly linked materials.

Similarly, nodes best positioned to influence the entire network can be identified using closeness cen-

trality. It measures how close a node is to all other nodes in terms of shortest path lengths. Higher values indicate nodes that can efficiently interact with the rest of the network. The average closeness centrality for materials is relatively low (0.101), reflecting the sparse and fragmented nature of the network. Motifs with high closeness values are well-positioned in the network to connect different material families and help maintain the network's global connectivity. For example, materials MnWO_4 and WO_3 are connected through the common WO_6 motif, even though they have different structures. The peak at zero closeness reflects the presence of disconnected or weakly connected nodes due to the limited motif overlap across materials.

Betweenness centrality quantifies how often a node lies on the shortest paths between other nodes, identifying potential structural bridges between otherwise disconnected clusters in the network. The low average betweenness centrality (0.0002) for materials suggests that there are few nodes acting as structural bridges between materials that are otherwise disconnected in the network. For example, material BaSnO_3 acts as a bridge connecting materials sharing motifs BaO_{12} and SnO_6 , whereas motif MgBr_6 bridges materials MgBr_2 and Li_2MgBr_4 , which are structurally dissimilar. Such bridging materials and motifs are important in the network because they form structurally and functionally meaningful connections.

Together, these metrics suggest that the material connectivity in the network is mediated through a small number of structurally significant motifs. Motifs such as PO_4 , VO_4 , MnO_6 , WO_6 , and BaO_{12} not only define material clusters, but also bridge the network connecting materials with shared motifs. This enables the discovery of candidate materials for targeted applications defined by functional motifs.

3.2 Functional Applications Revealed by Motif Connectivity

The material-motif network provides a screening framework for identifying candidate compounds for targeted applications by exploiting connectivity through shared structural motifs. For motifs with known functionality, materials containing those motifs are collected, and an application-specific sub-network is constructed. Within each sub-network, clusters of previously studied materials are located, and their nearest neighbors within the same motif neighborhoods suggest additional candidate materials. Identified materials for solar cells, transparent conducting oxides (TCOs), superconductors, and battery electrodes are shown in **Figure 3**.

Motifs VO_4 tetrahedra, MnO_6 octahedra, and TiO_6 octahedra are studied for applications in solar energy conversion. Clusters of photovoltaic and photocatalytic materials emerge when these motif-based materials are linked by other functional motifs shown in Figure 3a (e.g., BiVO_4 , $\beta\text{-Mn}_2\text{V}_2\text{O}_7$ photoanodes and BaTiO_3 , TiO_2 , MnO_2 photocatalysts).[13, 14, 16, 47, 48, 49, 50, 51, 52, 53] The tetrahedral VO_4 motif forms a band-structure scaffold for modification by additional elements in ternary compounds. In BiVO_4 , hybridization between $\text{O}-2p$ and $\text{Bi}-6s$ states perturbs the $\text{V}-3d/\text{O}-2p$ manifold, tuning the valence band and bandgap to values suitable for photoanode application. Occurrence of these motifs across photoanodes and photocatalysts suggests that local structural units can be reused as practical design rules for optoelectronic function. The similar motif-based design rules can be used to screen candidate materials for photodetectors and transparent conducting oxides.[53, 54, 55, 56, 57, 58, 59, 60, 61, 62]

TCOs are wide-band-gap oxides that combine high electrical conductivity with visible transparency and are used in optoelectronic devices, including solar cells, light-emitting diodes, and optical sensors. In these materials, structure-property relations are governed by specific coordination motifs. For example, in the perovskite BaSnO_3 , the BaO_{12} motif with corner-sharing SnO_6 octahedra produces a highly dispersive $\text{Sn}-5s$ conduction band, while La substitution on Ba yields high room-temperature electron mobility.[50, 63] Similarly, in SnO , the $\text{Sn}^{2+} 5s^2$ lone pair hybridizes with $\text{O}-2p$ states to generate a dispersive valence band that enables *p*-type transparency.[64] These structure motifs provide a clear framework for selecting materials that can be used as transparent electrodes for LEDs, photovoltaics, and sensors.[48, 49, 50, 55, 63, 64, 65, 66, 67, 68, 69, 70, 71, 72, 73, 74, 75, 76]

In superconducting materials, clusters of iron pnictides are centered around motif FeAs_4 tetrahedral

motif (e.g., LaFeAsO , BaFe_2As_2).[17, 77, 78, 79, 80, 81] Hybridization between transition-metal d and anion p states in these motifs generates correlated electronic states that are characteristic of unconventional superconductivity in superconducting materials. Similarly, in cuprates (e.g., $\text{YBa}_2\text{Cu}_3\text{O}_7$), the CuO_2 planes including CuO_4 square-planar units are key motifs associated with superconductivity.[15, 82, 83, 84] In addition, distorted CuO_6 octahedra, as in La_2CuO_4 , strongly influence superconducting properties through octahedral tilts and bond-length distortions that modulate the Cu–O orbital overlap recognized in the discovery of high- T_c cuprates.[84, 85] These motifs act as structural blocks of superconducting layers, linking together distinct material families through shared motif-driven physics.

For rechargeable battery electrodes, motifs such as layered NaO_6 and MnO_6 octahedra, together with frameworks incorporating PO_4 tetrahedra, are observed across cathode materials.[86, 87, 88, 89, 90] The octahedral environments, as found in NaFePO_4 , NaCoO_2 , and substituted NaMnO_2 compounds, facilitate two-dimensional alkali-ion transport critical for high rate performance.[91, 92, 93] Polyanion-based systems such as $\text{Li}_3\text{V}_2(\text{PO}_4)_3$ and sodium superionic conductors (NASICONs; general formula $\text{Na}_x\text{M}_2(\text{PO}_4)_3$), derive their stability and higher redox potentials from the inductive effects of corner-sharing PO_4 units.[89, 90] These motifs thus encode the essential structural principles that control ion mobility, voltage, and cycling stability across both Li- and Na-ion electrode families.

Exploring the network along such motif connections allows for screening of materials structurally analogous to known functional compounds. The shared motifs define common atomic environments that unify otherwise distinct chemical families, pointing to candidates with multifunctional or tunable properties. For materials design, motif connectivity provides a practical route to candidate discovery: starting from a motif associated with a target property, one can follow explicit *material–motif–material* paths to identify additional materials that host the same structure motifs. The material–motif network is thus useful for functional materials discovery using motifs as intermediate steps in the screening process.

3.3 Material Embeddings Based on Material-Motif Bipartite Network

Structure motif-based bipartite networks use motif connectivity to assess material similarity. In the network representation, each material is linked to its constituent motifs, so the local coordination environments are tied directly to specific compounds. Two materials are related when they share one or more motifs, though the strength of that relation depends on the geometric distortions and frequency of the motif. Distortions are encoded as edge weights, which sharpen material–motif links beyond simple motif presence. Materials containing multiple motifs can bridge otherwise separate regions of the graph, creating transitive relations that cluster compounds with similar local geometries or functions. This motif-derived connectivity can be converted into quantitative descriptors suitable for predictive modeling. The material-motif bipartite network is embedded into a continuous vector space and the resulting material embeddings are used to assess the utility of this framework for motif-informed material descriptors and property prediction.

The Bipartite Network Embedding (BiNE) model[27] is adopted, which jointly optimizes two objectives: (1) preserving explicit material–motif associations via Kullback–Leibler (KL) divergence, and (2) capturing implicit transitive relations among materials mediated by shared motifs. A schematic workflow of the embedding procedure and the downstream property-prediction task is shown in **Figure 4**. Embeddings are updated using neighbor nodes under both objectives. The first-order neighbors of each material node are determined by its indirect connections to other materials linked by the same motifs. Initial node features are constructed as follows: materials are represented by one-hot atomic composition vectors, while motifs are encoded by concatenating motif type one-hot vectors with one-hot atomic vectors. These features are input to the BiNE model to learn vector representations (embeddings) of both materials and motifs. During training of explicit relations, motif site fingerprints are also used as features for motifs, as the same motif can exhibit different distortions across materials, captured by their fingerprints. The learned embeddings from the network map each node to a high-dimensional vector that captures both

explicit material–motif associations and implicit transitive relationships essential for identifying structural similarity and trends in material properties. The resulting node embeddings are later used for downstream tasks such as predicting material properties.

The learned material embeddings are used as input features for neural network models that predict formation energy, bandgap, and metal–nonmetal classification. Network-generated embeddings are obtained for Materials Project (MP) materials and for perovskite materials from the Matbench dataset to evaluate predictive performance across datasets. For the regression tasks (formation energy and bandgap), mean squared error (MSE) loss is used for training. Train–validation–test splits of 70:15:15 (formation energy) and 80:10:10 (bandgap) are used for model development and evaluation. In the embedding stage, the implicit objective uses first-order same-type neighborhoods (materials connected through shared motifs) to define training contexts, because these neighbors represent direct motif-mediated structural similarity. During implicit optimization, only material embeddings are updated to reflect the goal of learning material representations from motif connectivity.

After filtering the MP-derived dataset by property availability, 129,536 materials have formation energy labels and 130,548 have bandgap labels. The Mean Absolute Error (MAE) for formation energy prediction is $0.157 \text{ eV atom}^{-1}$, and for bandgap prediction 0.601 eV (**Table 2**), and the combined (implicit + explicit) embeddings improve over the implicit-only and explicit-only baselines. This trend indicates that both material–motif associations and motif-mediated transitive material–material relations contribute to the learned representations used for prediction. For a network generated using the Matbench perovskites dataset, which is dominated by octahedral and cuboctahedral motifs, the MAE for formation energy prediction is $0.164 \text{ eV atom}^{-1}$ (**Table 3**).

A binary classification task that classifies materials as metals or non-metals is also evaluated using the cross-entropy loss. This classification is useful for materials screening in applications that require either conducting or insulating behavior. The bipartite network yields 84% accuracy using combined relations, outperforming the implicit (72%) and explicit embeddings (74%).

Comparing the performance metrics, embeddings from the combined relations show improved results over both implicit-only and explicit-only embeddings (Table 2). For the bipartite network, both the formation energy and bandgap MAEs are lower for the combined relations than for the implicit and explicit baselines. This indicates that explicit material–motif links and implicit transitive relations capture complementary information: the explicit relation preserves motif-specific coordination environments, while implicit or transitive connectivity links materials through shared motifs. In addition to representations that focus primarily on composition and bonding, the motif-informed embeddings add an interpretable description of local coordination environments that is transferable across chemically distinct material families. Although state-of-the-art crystal graph models can achieve lower errors on these benchmarks, the goal is to establish motif connectivity as a complementary method for screening and structure–property learning, particularly when structure motifs are expected to play an important role in material properties. Property prediction becomes challenging as the dataset becomes more diverse, with sparsity in the network leading to outliers. These outliers underscore the need for incorporating higher-level atomic bonding and orbital information to improve the predictive accuracy. Future work could incorporate additional atomic-level details, such as bonding and orbital features, to address the remaining challenges, particularly for properties such as bandgap.

4 Conclusion

In summary, a bipartite network representation of materials and their structure motifs is introduced that captures both explicit relationships between materials and their structure motifs and transitive relationships among materials through shared motifs. Centrality analysis reveals that, despite the sparsity of the network, motif-sharing patterns contribute to formation of material clusters, supporting the role

of motifs as fundamental building blocks in materials. Clusters defined by functional motifs associated with different applications allow for expansion of the searchable material space to a large set of candidate materials. This framework can be used as an intermediate step in high-throughput materials discovery, enabling deeper exploration of the structure–property relationships in materials. Knowledge of functional motif driven material discovery can be a key input for designing materials with targeted properties.

Embeddings learned from the network based on motif connectivity provide improved predictive performance for material properties including formation energy, bandgap, and metal–nonmetal classification, outperforming models based solely on implicit or explicit relationships. These findings highlight the effectiveness of motif-centric embeddings for structure–property prediction and suggest that they can serve as feature vectors for materials. Incorporating additional atomic-scale features could further enhance model performance, particularly for electronic properties sensitive to local bonding and orbital character.

Supporting Information

Supporting Information is available from the Wiley Online Library or from the author.

Acknowledgements

We acknowledge funding support from the U.S. Department of Energy, Office of Science, Basic Energy Sciences, under Award No. DE-SC0023664. This research used resources of the National Energy Research Scientific Computing Center (NERSC), a U.S. Department of Energy Office of Science User Facility located at Lawrence Berkeley National Laboratory, operated under Contract No. DE-AC02-05CH11231 using NERSC award BES-ERCAP0029544.

References

- [1] A. Jain, S. P. Ong, G. Hautier, W. Chen, W. D. Richards, S. Dacek, S. Cholia, D. Gunter, D. Skinner, G. Ceder, et al., *APL materials* **2013**, *1*, 1.
- [2] S. Curtarolo, W. Setyawan, G. L. Hart, M. Jahnatek, R. V. Chepulskii, R. H. Taylor, S. Wang, J. Xue, K. Yang, O. Levy, et al., *Computational Materials Science* **2012**, *58* 218.
- [3] J. E. Saal, S. Kirklin, M. Aykol, B. Meredig, C. Wolverton, *Jom* **2013**, *65* 1501.
- [4] G. Bergerhoff, I. Brown, F. Allen, et al., *International Union of Crystallography, Chester* **1987**, *360* 77.
- [5] C. Lang, Z. Wang, K. He, S. Sun, *The Journal of Supercomputing* **2022**, *78*, 7 9782.
- [6] J.-Y. Li, J. Teng, H. Wang, *Physica A: Statistical Mechanics and its Applications* **2023**, *628* 129169.
- [7] A. Kopsidas, K. Kepaptsoglou, *Journal of Complex Networks* **2024**, *12*, 1 cnad050.
- [8] G. A. Pavlopoulos, P. I. Kontou, A. Pavlopoulou, C. Bouyioukos, E. Markou, P. G. Bagos, *GigaScience* **2018**, *7*, 4 giy014.
- [9] D. E. Hostallero, Y. Li, A. Emad, *Bioinformatics* **2022**, *38*, 14 3609.
- [10] O. Isayev, D. Fourches, E. N. Muratov, C. Oses, K. Rasch, A. Tropsha, S. Curtarolo, *Chemistry of Materials* **2015**, *27*, 3 735.
- [11] M. Aykol, V. I. Hegde, L. Hung, S. Suram, P. Herring, C. Wolverton, J. S. Hummelshøj, *Nature communications* **2019**, *10*, 1 2018.
- [12] A. Veremyev, L. Liyanage, M. Fornari, V. Boginski, S. Curtarolo, S. Butenko, M. Buongiorno Nardelli, *AIChe Journal* **2021**, *67*, 3 e17051.

[13] A. Elaouni, M. El Ouardi, A. BaQais, M. Arab, M. Saadi, H. Ait Ahsaine, *RSC advances* **2023**, *13*, 26 17476.

[14] F. Xu, B. Weng, *Journal of Materials Chemistry A* **2023**, *11*, 9 4473.

[15] D. Pelc, R. J. Spieker, Z. W. Anderson, M. J. Krogstad, N. Biniskos, N. Bielinski, B. Yu, T. Sasagawa, L. Chauviere, P. Dosanjh, et al., *Scientific reports* **2022**, *12*, 1 20483.

[16] Z. Meng, H. Yan, P. Qin, X. Zhou, X. Wang, H. Chen, L. Liu, Z. Liu, *Advanced Functional Materials* **2023**, *33*, 46 2305225.

[17] G. Stewart, *Reviews of Modern Physics* **2011**, *83*, 4 1589.

[18] N. E. Zimmermann, M. K. Horton, A. Jain, M. Haranczyk, *Frontiers in Materials* **2017**, *4* 34.

[19] N. E. Zimmermann, A. Jain, *RSC advances* **2020**, *10*, 10 6063.

[20] D. Waroquiers, X. Gonze, G.-M. Rignanese, C. Welker-Nieuwoudt, F. Rosowski, M. Göbel, S. Schenk, P. Degelmann, R. André, R. Glaum, et al., *Chemistry of Materials* **2017**, *29*, 19 8346.

[21] S. P. Ong, W. D. Richards, A. Jain, G. Hautier, M. Kocher, S. Cholia, D. Gunter, V. L. Chevrier, K. A. Persson, G. Ceder, *Computational Materials Science* **2013**, *68* 314.

[22] B. Perozzi, R. Al-Rfou, S. Skiena, In *Proceedings of the 20th ACM SIGKDD international conference on Knowledge discovery and data mining*. **2014** 701–710.

[23] A. Grover, J. Leskovec, In *Proceedings of the 22nd ACM SIGKDD international conference on Knowledge discovery and data mining*. **2016** 855–864.

[24] Y. Dong, N. V. Chawla, A. Swami, In *Proceedings of the 23rd ACM SIGKDD international conference on knowledge discovery and data mining*. **2017** 135–144.

[25] W. Huang, Y. Li, Y. Fang, J. Fan, H. Yang, In *Proceedings of the 43rd international ACM SIGIR conference on research and development in information retrieval*. **2020** 149–158.

[26] A.-L. Barabasi, Z. N. Oltvai, *Nature reviews genetics* **2004**, *5*, 2 101.

[27] M. Gao, L. Chen, X. He, A. Zhou, In *The 41st international ACM SIGIR conference on research & development in information retrieval*. **2018** 715–724.

[28] J. Sybrandt, I. Safro, *arXiv preprint arXiv:1905.10953* **2019**.

[29] S. Athar, R. A. Abbasi, Z. Saeed, A. Said, I. Razzak, F. D. Salim, *World Wide Web* **2023**, *26*, 5 3463.

[30] T. Xie, J. C. Grossman, *Physical review letters* **2018**, *120*, 14 145301.

[31] C. Chen, W. Ye, Y. Zuo, C. Zheng, S. P. Ong, *Chemistry of Materials* **2019**, *31*, 9 3564.

[32] Y. Dong, C. Wu, C. Zhang, Y. Liu, J. Cheng, J. Lin, *npj Computational Materials* **2019**, *5*, 1 26.

[33] S. Gong, T. Xie, T. Zhu, S. Wang, E. R. Fadel, Y. Li, J. C. Grossman, *Physical Review B* **2019**, *100*, 18 184103.

[34] C. W. Park, C. Wolverton, *Physical Review Materials* **2020**, *4*, 6 063801.

[35] K. Choudhary, B. DeCost, *npj Computational Materials* **2021**, *7*, 1 185.

[36] R. Ruff, P. Reiser, J. Stühmer, P. Friederich, *Digital Discovery* **2024**, *3*, 3 594.

[37] H. R. Banjade, S. Hauri, S. Zhang, F. Ricci, W. Gong, G. Hautier, S. Vucetic, Q. Yan, *Science advances* **2021**, *7*, 17 eabf1754.

[38] Z. Yu, H. Gao, In *International Conference on Machine Learning*. PMLR, **2022** 25581–25594.

[39] M. Pinsky, D. Avnir, *Inorganic chemistry* **1998**, *37*, 21 5575.

[40] J. Lima-de Faria, E. Hellner, F. Liebau, E. Makovicky, E. Parthé, *Acta Crystallographica Section A: Foundations of Crystallography* **1990**, *46*, 1 1.

[41] A. Hagberg, D. Conway, *URL: <https://networkx.github.io>* **2020**.

[42] M. Bastian, S. Heymann, M. Jacomy, In *Proceedings of the international AAAI conference on web and social media*, volume 3. **2009** 361–362.

[43] P. Shannon, A. Markiel, O. Ozier, N. S. Baliga, J. T. Wang, D. Ramage, N. Amin, B. Schwikowski, T. Ideker, *Genome research* **2003**, *13*, 11 2498.

[44] I. E. Castelli, D. D. Landis, K. S. Thygesen, S. Dahl, I. Chorkendorff, T. F. Jaramillo, K. W. Jacobsen, *Energy & Environmental Science* **2012**, *5*, 10 9034.

[45] B. Khorsand, A. Savadi, M. Naghibzadeh, *BMC bioinformatics* **2020**, *21* 1.

[46] A.-L. Barabási, *Philosophical Transactions of the Royal Society A: Mathematical, Physical and Engineering Sciences* **2013**, *371*, 1987 20120375.

[47] Q. Yan, J. Yu, S. K. Suram, L. Zhou, A. Shinde, P. F. Newhouse, W. Chen, G. Li, K. A. Persson, J. M. Gregoire, et al., *Proceedings of the National Academy of Sciences* **2017**, *114*, 12 3040.

[48] P. Dhull, A. Sudhaik, V. Sharma, P. Raizada, V. Hasija, N. Gupta, T. Ahamed, V.-H. Nguyen, A. Kim, M. Shokouhimehr, et al., *Molecular Catalysis* **2023**, *539* 113013.

[49] M. K. Hassan, M. T. Karim, D. Howlader, M. M. Alam, A. Kumer, *Heliyon* **2023**, *9*, 12.

[50] S. Jiao, J. Yan, G. Sun, Y. Zhao, *Journal of Semiconductors* **2016**, *37*, 7 072001.

[51] L. E. Navarrete-Cevallos, R. Vargas, P. J. Espinoza-Montero, *npj Clean Water* **2025**, *8*, 1 87.

[52] J. L. Da Silva, Y. Yan, S.-H. Wei, *Physical review letters* **2008**, *100*, 25 255501.

[53] Y. K. de Souza França, K. S. Pereira, Y. H. C. Feitosa, V. B. Marques, D. R. de Souza, *Orbital: The Electronic Journal of Chemistry* **2025**, 355–381.

[54] B. O’regan, M. Grätzel, *nature* **1991**, *353*, 6346 737.

[55] K. Ellmer, *Nature Photonics* **2012**, *6*, 12 809.

[56] S. Abbas, M. Kumar, J. Kim, *Materials Science in Semiconductor Processing* **2018**, *88* 86.

[57] N. Saxena, S. Sharma, P. Kumar, In *Metal Oxides for Next-Generation Optoelectronic, Photonic, and Photovoltaic Applications*, 277–300. Elsevier, **2024**.

[58] A. Al Miad, S. P. Saikat, M. K. Alam, M. S. Hossain, N. M. Bahadur, S. Ahmed, *Nanoscale Advances* **2024**, *6*, 19 4781.

[59] H. Tsubota, A. Jitianu, G. Kawamura, *ACS Materials Letters* **2025**, *7*, 3 1042.

[60] M. Deng, X. Fang, *Accounts of Materials Research* **2025**, *6*, 5 615.

[61] D. Nematov, A. Ashurov, M. Umarzoda, *Preprints* **2024**.

[62] M. Nadolska, M. Szkoda, K. Trzciński, P. Niedziałkowski, J. Ryl, A. Mielewczyk-Gryń, K. Górnicka, M. Przeoniak-Welenc, *Inorganic Chemistry* **2022**, *61*, 25 9433.

[63] H. J. Kim, U. Kim, T. H. Kim, H. S. Mun, B.-G. Jeon, K. T. Hong, W.-J. Lee, C. Ju, K. H. Kim, K. Char, et al., *Applied Physics Express* **2012**, *5*, 6 061102.

[64] Q. Xu, Y. Li, L. Zhang, W. Zheng, D. J. Singh, Y. Ma, *Chemistry of Materials* **2017**, *29*, 6 2459.

[65] R. Woods-Robinson, M. Morales-Masis, G. Hautier, A. Crovetto, *PRX Energy* **2024**, *3*, 3 031001.

[66] J. Morales-Bautista, H. Guillén-Bonilla, L. I. Juárez-Amador, A. Guillén-Bonilla, V.-M. Rodríguez-Betancourt, J. A. Ramírez-Ortega, J. T. Guillén-Bonilla, M. d. l. L. Olvera-Amador, *Chemosensors* **2025**, *13*, 9 329.

[67] I. Khan, A. Z. Khan, A. Sufyan, M. Y. Khan, S. I. Basha, A. Khan, *Ultrasonics Sonochemistry* **2020**, *68* 105233.

[68] J. Zeng, H. Wang, Y. Zhang, M. K. Zhu, H. Yan, *The Journal of Physical Chemistry C* **2007**, *111*, 32 11879.

[69] H. Wen, B. Weng, B. Wang, W. Xiao, X. Liu, Y. Wang, M. Zhang, H. Huang, *Nanomaterials* **2024**, *14*, 7 591.

[70] G. Brunin, F. Ricci, V.-A. Ha, G.-M. Rignanese, G. Hautier, *npj Computational Materials* **2019**, *5*, 1 63.

[71] S. Calnan, A. Tiwari, *Thin solid films* **2010**, *518*, 7 1839.

[72] J. Kim, H. Yun, J. Seo, J. H. Kim, J. H. Kim, K. A. Mkhoyan, B. Kim, K. Char, *ACS Applied Electronic Materials* **2022**, *4*, 7 3623.

[73] J. Zhang, B. Li, C. Xia, G. Pei, Q. Deng, Z. Yang, W. Xu, H. Shi, F. Wu, Y. Wu, et al., *Journal of Physics and Chemistry of Solids* **2006**, *67*, 12 2448.

[74] Z. Zhang, P. Yan, Q. Song, H. Chen, W. Zhang, H. Yuan, F. Du, D. Liu, D. Chen, Y. Zhang, *Fundamental Research* **2024**, *4*, 5 1292.

[75] A. Stadler, *Materials* **2012**, *5*, 4 661.

[76] A. Walsh, Y. Yan, M. N. Huda, M. M. Al-Jassim, S.-H. Wei, *Chemistry of Materials* **2009**, *21*, 3 547.

[77] Y. Kamihara, T. Watanabe, M. Hirano, H. Hosono, *Journal of the American Chemical Society* **2008**, *130*, 11 3296.

[78] M. Rotter, M. Tegel, D. Johrendt, *Physical review letters* **2008**, *101*, 10 107006.

[79] F. Ma, Z.-Y. Lu, *Physical Review B—Condensed Matter and Materials Physics* **2008**, *78*, 3 033111.

[80] R. Sharma, In *Superconductivity: Basics and Applications to Magnets*, 313–353. Springer, **2021**.

[81] P. Dai, *Reviews of Modern Physics* **2015**, *87*, 3 855.

[82] F. Hunte, J. Jaroszynski, A. Gurevich, D. Larbalestier, R. Jin, A. Sefat, M. A. McGuire, B. C. Sales, D. K. Christen, D. Mandrus, *nature* **2008**, *453*, 7197 903.

[83] D. Zhang, C. Boffo, D. C. Dunand, *Nature communications* **2025**, *16*, 1 1933.

[84] B. Keimer, S. A. Kivelson, M. R. Norman, S. Uchida, J. Zaanen, *Nature* **2015**, *518*, 7538 179.

[85] J. G. Bednorz, K. A. Müller, *Zeitschrift für Physik B Condensed Matter* **1986**, *64*, 2 189.

[86] H. Wang, Y. Yang, Y. Liang, L.-F. Cui, H. S. Casalongue, Y. Li, G. Hong, Y. Cui, H. Dai, *arXiv preprint arXiv:1107.0111* **2011**.

[87] R. D. McAuliffe, G. E. Kamm, M. J. McDermott, R. P. Hermann, N. Vasquez-Garcia, R. L. Sacci, K. A. Persson, K. W. Chapman, G. M. Veith, *Inorganic Chemistry* **2023**, *62*, 8 3358.

[88] D. Nayak, P. K. Jha, S. Ghosh, V. Adyam, *Journal of Power Sources* **2019**, *438* 227025.

[89] T. Gavrilova, Y. Deeva, A. Uporova, T. Chupakhina, I. Yatsyk, A. Rogov, M. Cherosov, R. Batulin, M. Khrizanforov, S. Khantimerov, *International Journal of Molecular Sciences* **2024**, *25*, 5 2884.

[90] J. Wang, T. He, X. Yang, Z. Cai, Y. Wang, V. Lacivita, H. Kim, B. Ouyang, G. Ceder, *Nature communications* **2023**, *14*, 1 5210.

[91] N. Liu, B. Li, Z. He, L. Dai, H. Wang, L. Wang, *Journal of Energy Chemistry* **2021**, *59* 134.

[92] X. Chen, H. Zhang, J.-H. Liu, Y. Gao, X. Cao, C. Zhan, Y. Wang, S. Wang, S.-L. Chou, S.-X. Dou, et al., *Energy Storage Materials* **2022**, *50* 21.

[93] Q. Fu, J. Wang, A. Sarapulova, L. Zhu, A. Missyul, E. Welter, X. Luo, Z. Ding, M. Knapp, H. Ehrenberg, et al., *Journal of Materials Chemistry A* **2021**, *9*, 31 16776.

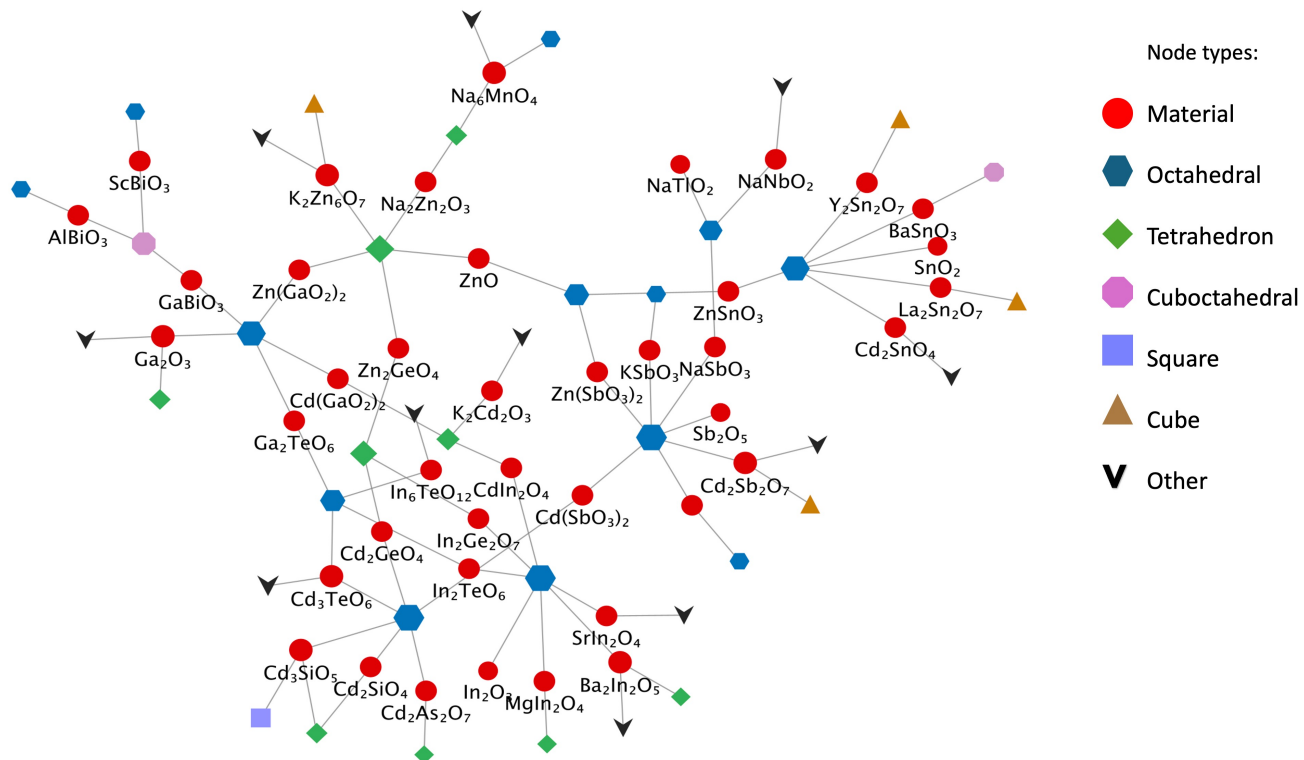


Figure 1. A sample network for a small set of complex metal oxides (red circular nodes) and their structure motifs with different motif types. Only most common motif types are shown and remaining ones are included as other types.

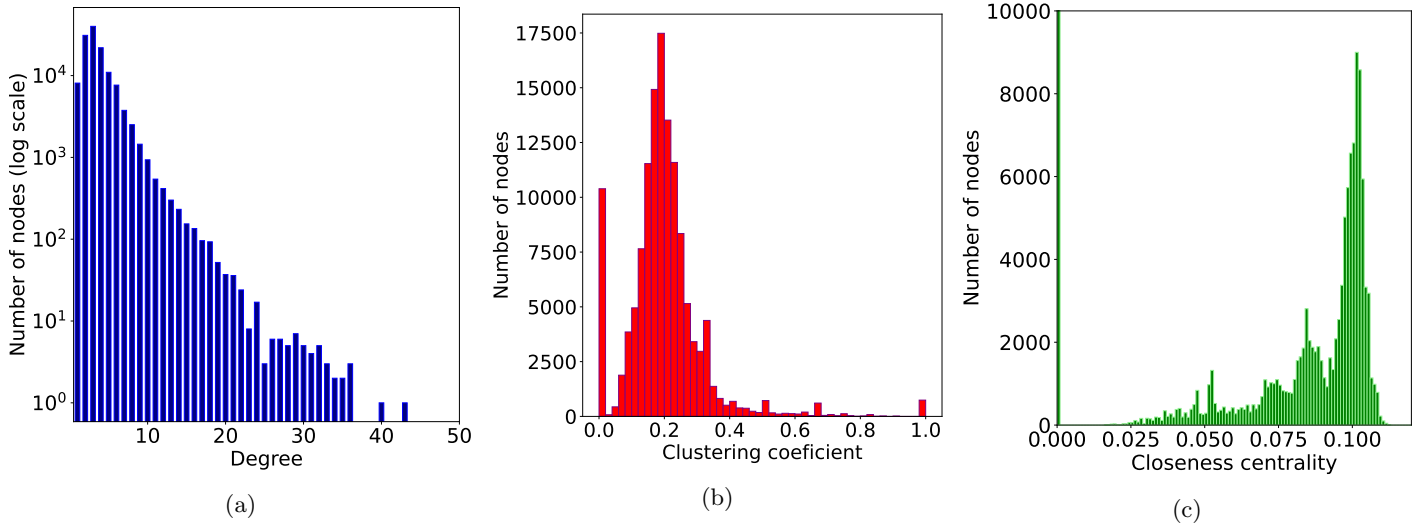


Figure 2. Centrality measures in network a) degree distribution, b) clustering coefficient and c) closeness centrality for material nodes in the network. Degree identifies highly recurrent motif hubs, moderate clustering reveals several local communities, and low average closeness indicates a sparse network in which only a small number of motifs and materials connect diverse material families.

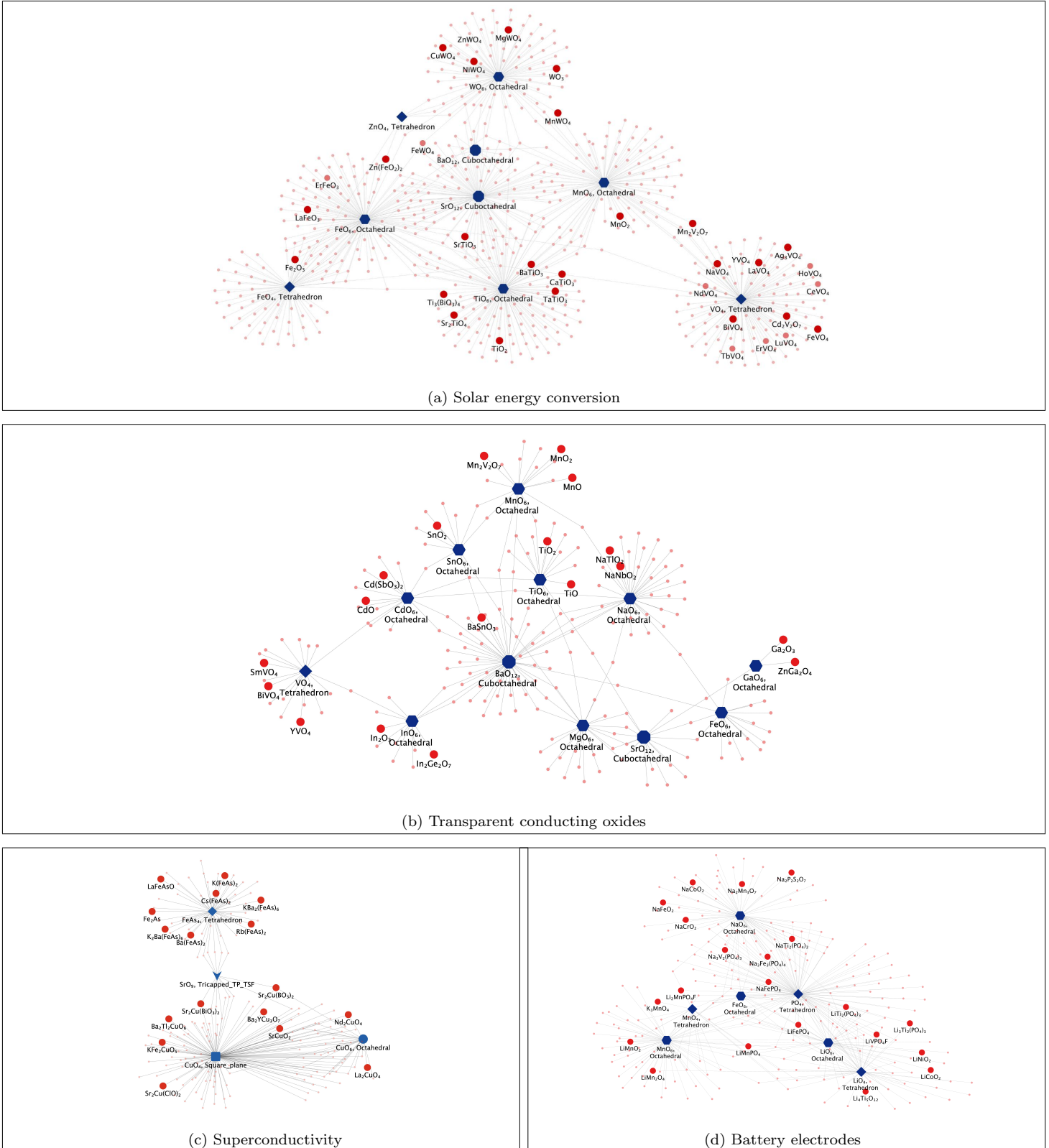


Figure 3. Sub-networks showing material clusters based on shared motifs for (a) solar energy conversion, (b) transparent conducting oxides, (c) superconductivity, and (d) battery electrodes. Motif nodes are shown in blue and material nodes in red. Each subgraph highlights representative materials previously studied for the indicated functionality and their associated motifs.

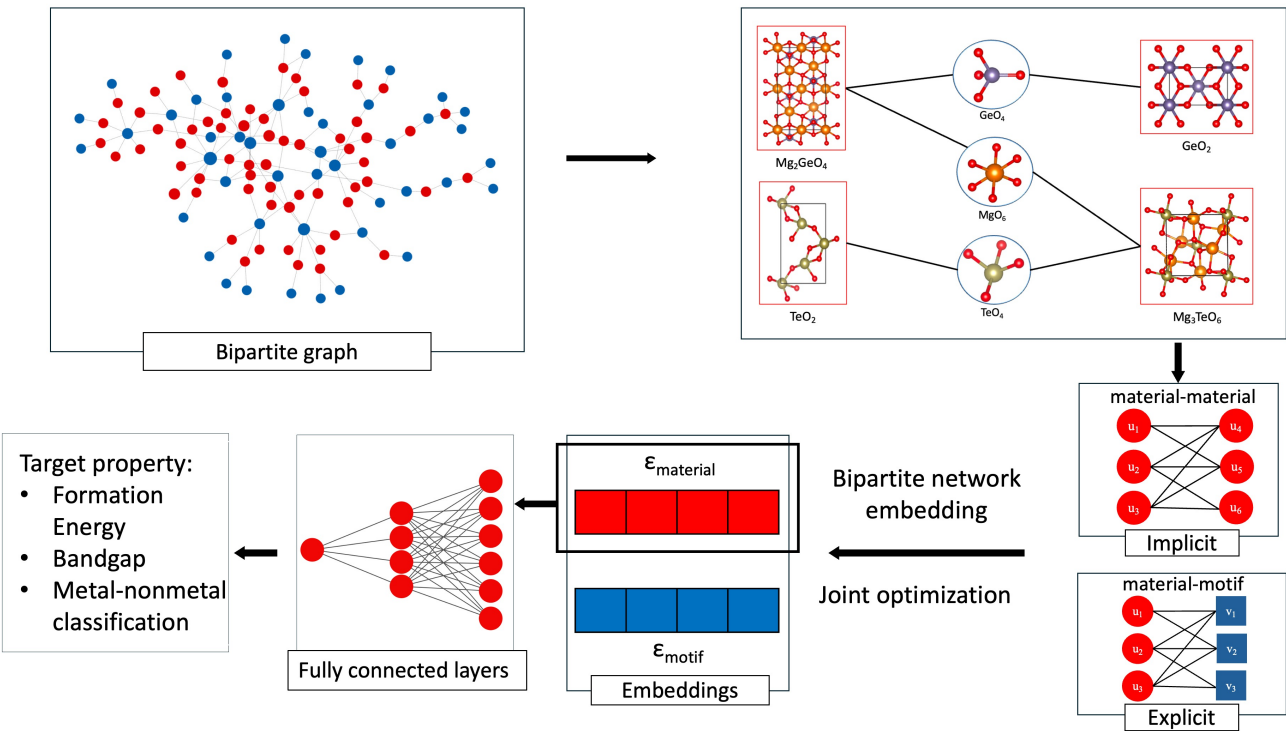


Figure 4. Schematic representation of the bipartite network embedding process and material property prediction. From material–motif bipartite graph, motif connectivity is used to explore material relationships. Embeddings are generated with BiNE using explicit and implicit objectives. The resulting material embeddings are then used for regression and classification tasks.

Table 1: Centrality measures for the networks studied. The material–motif networks show moderate clustering and low average betweenness, consistent with sparse connectivity with a small set of bridging nodes.

Network	Clustering coefficient	Betweenness centrality	Closeness centrality
Materials (MP database[1])	0.201	0.0002	0.101
Perovskites (Matbench[44])	0.300	0.0003	0.195
Human–virus PPI[45]	0.095	0.0002	0.320

Table 2: Property-prediction performance on Materials Project materials using learned material embeddings from material–motif network. Results are reported for combined (implicit and explicit), implicit-only, and explicit-only embeddings.

Metric	Combined (Implicit + Explicit)	Implicit	Explicit
Formation energy MAE (eV atom ⁻¹)	0.157	0.284	0.341
Bandgap MAE (eV)	0.601	0.649	0.673
Metal–nonmetal classification accuracy (%)	84%	72%	74%

Table 3: Formation energy prediction error (MAE) for perovskite subsets from the Materials Project and Matbench datasets using learned material embeddings.

Metric	Perovskites (MP database)	Perovskites (Matbench)
Formation energy MAE (eV atom ⁻¹)	0.171	0.164